

Statistical properties of H II regions in the disc of M100

J. H. Knapen

Department of Physical Sciences, University of Hertfordshire, Hatfield, Herts AL10 9AB, UK. E-mail knapen@star.herts.ac.uk

Accepted January 1998; Received; in original form

ABSTRACT

From a new mosaic image in the H α line of the complete disc of the spiral galaxy M100, a catalogue is composed listing 1948 individual H II regions. I give details of the data collection and reduction procedure, and of the production of the H II region catalogue. For each H II region, the catalogue gives its position relative to the centre of the galaxy, its deprojected distance to the centre, its radius, and its calibrated luminosity. An indication is included as to whether the H II region is located in the arms, between them, or in the circumnuclear star-forming region. I present the results of a statistical study of properties of the H II regions. The luminosity function of the complete ensemble of H II regions shows a characteristic shape well fitted by a power-law slope in the higher luminosity range, and complying with literature values for galaxies like M100. Luminosity function slopes for arm and interarm H II region populations separately are found to be equal within the errors of the fits, indicating that whereas the density wave accumulates material into the arm regions, and may trigger star formation there, it does not in fact change the mass distribution of the star-forming clouds, nor the statistical properties of the H II region population. Diameter distributions and the radial number density distribution are discussed. The latter indicates those areas where most star formation occurs: the circumnuclear region and the spiral arms. The huge number of H II regions allowed the construction of a number of independent luminosity functions at different distances to the nucleus. The slope of the luminosity function shows a marginal decrease with increasing distance from the centre, which could indicate a gradual change toward shallower IMF slopes with increasing galactocentric distance, or an evolutionary effect.

Key words: ISM: H II regions – galaxies: individual (M100, NGC 4321) – galaxies: ISM – galaxies: spiral – galaxies: structure

1 INTRODUCTION

H II regions in galaxies are formed when the neutral gas surrounding a region of massive star formation (SF) is being ionized by the ultraviolet radiation of the young stars within it. The absorbed radiation is emitted as a nebular emission line spectrum, with the H α line as its most powerful emission line in the optical range. Most H II regions are thought to be ionization bounded, in which case the luminosity in e.g. the H α line scales directly with the number of ionising photons (Kennicutt 1992), although the largest H II regions, at luminosities $L > 10^{38.7}$ erg s $^{-1}$, are probably density bounded (Beckman et al. 1998). The H α line is one of the most widely used lines to study massive SF in external galaxies due to the ease with which it can be measured over complete galactic discs.

Kennicutt, Edgar & Hodge (1989) studied H II region populations in a sample of 30 galaxies, ranging in morphological type from Sb to Irr. They constructed luminosity

functions (LFs) and found that these can be described by a power law function with $N(L) \propto L^{-2 \pm 0.5}$. H II regions are more prevalent in late type than in early type galaxies, and the LF is shallower in the former. Kennicutt et al. (1989) could construct separate arm and interarm LFs for five galaxies in their sample, and found that the interarm LF slope is significantly different from that of the arm LF.

In a series of papers, of which the present one forms part, we have described results from imaging spiral galaxies in the H α line using the 4.2m William Herschel Telescope (WHT). Deep images with superb spatial resolution allowed the creation of large catalogues of H II regions for individual galaxies, and a detailed study of their statistical properties. Cepa & Beckman (1989, 1990a) studied the distribution of H II regions in NGC 3992 and in the inner $3' \times 4'$ of M100. Knapen et al. (1993a) described a detailed study of the H II regions in NGC 6814, and Rozas, Beckman & Knapen (1996a) and Rozas, Knapen & Beckman (1996b)

arXiv:astro-ph/9801227v1 23 Jan 1998

studied NGC 157, NGC 3631, NGC 6764 and NGC 6951. This series of papers is complemented by the study of Rand (1992) of the H II regions in M51, which is based on an image of comparably good characteristics. LFs for all these galaxies can be fitted by power laws, complying with earlier work. Diameter and radial distributions also show few surprises. Significantly different slopes of arm and interarm LFs were only found in M51. Other recent H II region studies include those by Ryder & Dopita (1993) for nearby southern spirals, Hodge & Miller (1995) for local group galaxies, Tsvetanov & Petrosian (1995) for Seyfert galaxies, Crocker, Baugus & Buta (1996) for ringed galaxies, and Evans et al. (1996) and González Delgado et al. (1997) for AGN host galaxies. H II region studies have also been published for M100: Hodge & Kennicutt (1983) present positional data for 286 H II regions from a photographic image, used by Anderson, Hodge & Kennicutt (1983) to analyze aspects of the galaxy's spiral structure. Cepa & Beckman (1990a) catalogued 456 H II regions in the inner region of the disc of M100, Arsenault, Roy & Boulesteix (1990) measured parameters for 127 H II regions from an H α image obtained from their Fabry-Pérot data set, and Banfi et al. (1993) catalogued 83 H II regions from their H α image.

In the present paper, I use a new H α image of the complete disc of M100, at uniformly high spatial resolution, to construct a catalogue of almost 2000 individually measured H II regions, and to study basic statistical properties.

M100 (=NGC 4321) is a grand-design galaxy of type .SXS4.. (de Vaucouleurs et al. 1991) with a moderately strong bar. In previous papers, we have discussed the H I distribution and kinematics (Knapen et al. 1993b) and described CO measurements (Cepa et al. 1992; Knapen et al. 1996), which was combined with the H α image described in detail in the present paper to determine massive SF efficiencies in arm and interarm regions (Knapen et al. 1996). The galaxy has a circumnuclear region (CNR) of strongly enhanced SF, where a pair of miniature spiral armlets occurs in a resonance region between the inner and outer parts of the bar (Knapen et al. 1995a,b). I adopt a distance to M100 of $D = 16.1 \pm 1.3$ Mpc (Ferrarese et al. 1996). At this distance, 1'' corresponds to 78 ± 6 pc.

The structure of this paper is as follows. The observations and data reduction procedures are described in Section 2. The H α image of M100 and the production of the catalogue of H II regions based upon it is discussed in Section 3. Sections 4 and 5 are dedicated to the analysis of the catalogue, dealing with the luminosity and geometrical distribution and how these change over the disc surface. The main conclusions are discussed in a wider context of SF processes in galactic discs and summarized in Section 6.

2 OBSERVATIONS AND DATA REDUCTION

The H α image of M100 was obtained during two observing runs with the 4.2 m WHT on La Palma, using the TAURUS camera in imaging mode. Since the field of view in this setup is limited by the filter size to around 5' diameter, four fields of the galaxy were imaged, two (eastern half of M100) during the night of 27 May 1991, and two (western half) during the night of 14 March 1992.

Narrow band redshifted H α filters with width of 15Å

were used for the observations, centred at $\lambda_c = 6601\text{Å}$ for the H α line observations (redshifted using the galaxy's systemic velocity $v_{\text{sys}} = 1571 \text{ km s}^{-1}$; Knapen et al. 1993b) and at $\lambda_c = 6577\text{Å}$ and 6565Å for the continuum. Exposure times were 1200 seconds for both the on-line and the continuum image on the first night, and 2×900 seconds on the second night. An EEV CCD chip was used during both observing runs, with a projected pixel size of $0''.279$, and a size of 1180×1280 pixels.

For both observing runs, the images were first bias-subtracted and flat-fielded in a standard way. Use of dawn and dusk flatfields gave satisfactory results, but some interference fringes are present at low levels in the two eastern frames. The residual variations in background level due to this are at most of order 10 counts. Compared with the minimum ($= 3\sigma$) value of around 120 in each pixel to be included in a catalogued H II region (see below), the resulting error in the H II region flux is always smaller than $\sim 10\%$, and only approaches 10% for the smallest and faintest regions. After flat-fielding, a sky background estimate was made by measuring the levels and r.m.s. fluctuations in areas of the images which are free of galaxy emission. Since in each exposure the centre of the galaxy is in one of the corners of the chip, it was always possible to find sufficiently large areas to determine a reliable sky value. Subtracted sky values ranged from 750 to 1000 counts in the four (two on- plus two off-line) eastern images, and from 150 to 500 counts in the eight western images. The lower sky values in the latter images are due to shorter exposure times, and a different position of the moon (which was setting). Note that lower sky background values result in lower residual noise in the final H α images.

The on- and off-line images were aligned to better than 0.2 pixel using fits to positions of foreground stars. These fits were also used to check and confirm that the seeing did not change within each set of images that were to be combined. Cosmic rays were removed from the eastern images by hand, where pixels affected by cosmic ray hits were removed and replaced by the average value of a number of neighbouring pixels. In the case of the western exposures, where sets of two images at the same position, and imaged through the same filter, were available, cosmic ray hits could be removed automatically by comparing the values of identical pixels in each set of images, and replacing unexpectedly high pixel values by an average of their neighbour's values. Comparison of the manual and automatic removal methods showed that both yield completely comparable and acceptable results. Almost all cosmic ray hits were removed, but a few dubious cases ($\ll 1\%$ of the number of unambiguously identified H II regions) were marked as such and discarded in the further analysis.

One curious linear feature which is not part of the galaxy is seen at position $\text{RA} \sim 12^{\text{h}} 20^{\text{m}} 29^{\text{s}}$, $\delta \sim 16^\circ 5'$. At low levels, it can be traced for some three minutes of arc. It is almost certainly due to a meteor which burned in the earth's atmosphere while the exposure was taken.

After aligning and cleaning the images, the continuum image was subtracted from the H α +continuum image taken at the same position. Following the same procedure as described by Knapen et al. (1993a) for NGC 6814, it was found that no scaling of the continuum images was necessary. This is because pairs of images were taken through filters with

very similar bandwidths and transmissions and in practically the same observing conditions.

At this stage there are four sub-images of M100, with the central region of the galaxy in another corner of the sub-image in each case. The properties (seeing, noise, etc.) are slightly different for each of the four, as summarized in Table 1. I used the four separate sub-images to catalogue the H II regions, and subsequently combined the four sub-catalogues into the master catalogue, as described in detail below. The sub-image with the best angular resolution is the one of the SE part of disc, and the H α image of the CNR as discussed in detail by Knapen et al. (1995a,b) was copied from that SE sub-image. A complete image of the disc of M100 was also produced, and is shown in Fig. 1. Note that this is the image that has been used to study massive SF efficiencies by Knapen et al. (1996) and to study the disc morphology and relations between stars, gas and dust by Knapen & Beckman (1996).

The four individual sub-images were combined into one mosaic as follows. For the geometrical calibration, the sub-images were aligned by determining the positions of the centre, residuals of field stars, and strong, compact H II regions. Photometric calibration was available for the two nights during which the observations were taken, but was more reliable for the 1992 run. The sub-images were scaled relatively by determining total fluxes in certain well-defined regions, e.g. the whole of the central region, or parts of the spiral arms. I used several areas per pair of images considered, and found consistent results in all cases. The error in this relative calibration is estimated to be $< 2.5\%$. This is smaller than the error in the photometric calibration, but in any case the dominant errors in the absolute calibration are the uncertainties in the distance to the galaxy and in the flux measurements of the individual H II regions. After convolving three of the sub-images with a Gaussian to the spatial resolution of the SW sub-image (Table 1), the sub-images were combined into the mosaic frame, taking into account the geometrical and calibration offsets described above. To obtain the absolute astrometric calibration, positions of foreground stars and the centre in the image were combined with their positions as listed in the Hubble Space Telescope Guide Star Catalog. The resulting image covers the complete disc of M100, with a constant spatial resolution of $1''.0 \times 1''.0$, and a pixel scale of $0''.279$.

From the photometric calibration obtained during the 1992 run, one instrumental count in the image was found to correspond to a luminosity of 3.78×10^{33} erg/s. This is assuming the Cepheid distance to M100 of 16.1 Mpc (Ferrarese et al. 1996). Note that the uncertainty given for this distance (of ± 1.3 Mpc) corresponds to an uncertainty of $\pm 0.55 \times 10^{33}$ erg/s per instrumental count in the calibration.

3 THE H II REGION CATALOGUE

In the production of the H II region catalogue for M100, I followed the procedures set out before by Knapen et al. (1993a) and Rozas et al. (1996a). Here, I briefly outline the main points, and indicate changes with respect to the previous work. A first difference to note is that for M100 I made separate H II region catalogues for the four sub-images, and

only at a later stage combined these lists, rather than measure all H II regions from the final, combined image.

A first step is the flagging of foreground stars in the H α images. This is easily done by comparison of the H α and continuum images, since stars will show comparable emission in these two, H II regions, however, relatively more in H α . This step prevents remnants of star images in the H α image to be falsely classified as H II regions. Building on our experience from previous work, I used as a selection criterion for H II regions that these should consist of at least nine contiguous pixels, each with an intensity of at least three times the r.m.s. noise level of the local background. Table 1 lists the r.m.s. noise of the background-subtracted H α images, and the lower limit cutoff in the H II region luminosities (determined by multiplying the minimum number of 9 pixels, the minimum count level of 3σ , and the calibration constant), for each of the four sub-images. The smallest catalogued regions are 3 pixels across, and thus have a physical diameter of some 65 pc. Note that the detection limit for H II regions is not constant over the whole disc due to the differences in background noise in the four sub-images. This has been taken into account later by not fitting slopes to LFs to points below the highest cutoff level.

After manually identifying each H II region, I measured its position in the image frame and its radius. The flux of each H II region was determined by integrating counts within a circular aperture. Sky subtraction errors, or errors due to local variations in the level can influence the luminosity determinations by no more than about 10% in even the weakest regions (see also Sect. 2), and by a few percent in most cases.

As discussed previously (Knapen et al. 1993a), there are possible complications in defining the H II regions and their extent due to a) H II regions partly or completely overlapping each other (as before, each significant peak was counted as a separate H II region as long as the peaks were separated by $> 3\sigma$); b) H II regions not being perfectly circular; and c) H II regions having ill-defined edges as a result of diffuse H α emission. Rand (1992) modelled the effects of a) on the LF of M51, and concluded that this factor is not a significant one in determining the true LF. I took care of b) wherever possible by slightly adjusting the aperture over which the flux was integrated. Finally, c) may have a slight impact on the determination of diameters of isolated H II regions, but given that edges are faint this will not significantly influence the determination of the LF. I thus conclude that the LF as determined from the catalogue will be a good approximation to the “true” LF.

Having constructed four separate LFs with information on the raw flux of all regions, the next step is to run a series of simple programs to produce the final, complete, catalogue, listing absolutely calibrated fluxes (calibration is slightly different for each sub-frame, as described in Sect. 2), and position from the centre of the galaxy rather than in the frame. Using values for the inclination angle of the galaxy of 27° and for the position angle of the major axis of 153° (Knapen et al. 1993b), deprojected distances from the centre were also calculated and listed. All the positions and distances are listed in seconds of arc, the calibrated fluxes in erg s^{-1} . Absolute positions of specific H II regions should be correct to within $\sim 2''$, the accuracy of the absolute astrometry, but relative positions among H II regions should

Table 1. Properties of the four H α sub-images obtained of the disc of M100. Background noise, seeing and lower luminosity cutoff for the detection of H II regions are given in columns 3, 4, and 5

Sub-im.	Observed	Rms noise (instr. cnts.)	FWHM ($''$)	Cutoff (log of erg s^{-1})
NW	14 Mar 1992	43	$0''.8 \times 0''.8$	36.6
NE	27 May 1991	44	$1''.0 \times 0''.7$	36.7
SE	27 May 1991	45	$0''.75 \times 0''.65$	36.7
SW	14 Mar 1992	30	$1''.0 \times 1''.0$	36.5

be of much higher accuracy. I estimate the calibrated fluxes to be accurate to $\sim 10\%$ on an individual basis.

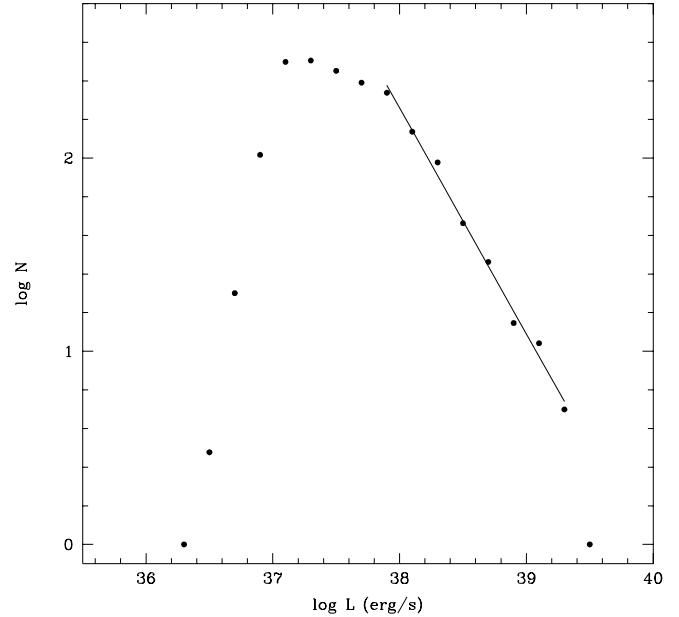
All H II regions in the catalogue were assigned to either arm or interarm parts of the disc, or to the CNR. I based most of this classification on the mask used by Knapen & Beckman (1996). I deviated from the mask only in the case of a string of H II regions in the bar region of M100, NW of the centre, which I classified as “arm”. Unfortunately, these H II regions are not sufficiently numerous to warrant construction of a separate LF for bar H II regions. In all, 1099 H II regions were assigned to the arms, 750 to the interarm regions, with 99 classified as forming part of the CNR. Note that the list of 750 interarm H II regions alone is several times longer than most lists of H II regions published in the literature for complete galaxy discs so far, with only a handful of longer lists available.

The final catalogue of H II regions has 1849 entries for the disc of M100, plus another 99 for the CNR, making a total of 1948. The complete list is published electronically through the CDS*, and is also available in electronic form from the author. Column 1 in the catalogue is the number assigned to the H II regions; columns 2 and 3 are the relative distances from the centre of the galaxy, in right ascension and declination, in arcsec; column 4 is the deprojected distance to the centre, in arcsec; column 5 the radius in arcsec; and column 6 the luminosity of the H II regions, in $10^{36} \text{ erg s}^{-1}$. Finally, column 7 gives the classification of the H II regions as arm (A), interarm (I) or CNR (C).

4 LUMINOSITY FUNCTIONS

4.1 Total LF

The LF of the H II regions in the disc of M100 was constructed using bins of 0.1 and 0.2 in the log of the luminosity, in order to check possible effects of the bin size on the LF shape. These effects were found to be very small, and not affecting the fit of the slope to the LF, the main parameter deduced from the LFs. I thus decided to follow the precedent set in the literature, and show only LFs with 0.2 bin. Fig. 2 shows the LF for the disc of the galaxy, but excluding the H II regions in the CNR (see below). The detection limit of individual H II regions of $\log L \sim 36.6 \text{ erg s}^{-1}$ is clearly visible in the LF as a drop on the low luminosity side. This

**Figure 2.** H II region LF for the disc of M100 (excluding the CNR). Bin size is 0.2 in the log of L . Line indicates best fit, and the range in $\log L$ over which the fit was made.

detection limit is slightly lower than that in Knapen et al. (1993a) and similar to those reported in Rozas et al. (1996a). The peak in the LF occurs around $\log L = 37.1 \text{ erg s}^{-1}$, again comparable to our previous studies. These similarities are of course a result of the equal observing techniques used in all cases, but do show the consistently high quality of the data.

I fitted a function of type $N(L) = A L^a dL$ to the high- L side of the LF, and determined a slope of the LF above $\log L = 37.9 \text{ erg s}^{-1}$ of $a = -2.17 \pm 0.04$. This slope is well within the usual range of LF slopes found for galaxies of similar morphological type (e.g. Kennicutt et al. 1989; Knapen et al. 1993a; Rozas et al. 1996a). Note that LF slopes for M100 in the literature range from -1.4 (Arsenault et al. (1990), via -2.1 (Banfi et al. 1993) to -2.7 (Cepa & Beckman 1990a), but are all based on data of much lower quality. The error on the fit to the slope is solely the error due to the least-squares fit to the data points. The size of the bins does not seem to be an important factor in the determination of the slope: fitting the slope (over the same range in $\log L$) to the LF constructed with bins of 0.1 gives $a = -2.16 \pm 0.04$. Including the H II regions in the CNR in the LF, predictably, lowers the slope to $a = -1.95 \pm 0.04$

* The H II region catalogue is available electronically from the Centre de Données astronomiques de Strasbourg (CDS), on: ftp://cdsarc.u-strasbg.fr/pub/cats/J/MNRAS/volume/first_page.

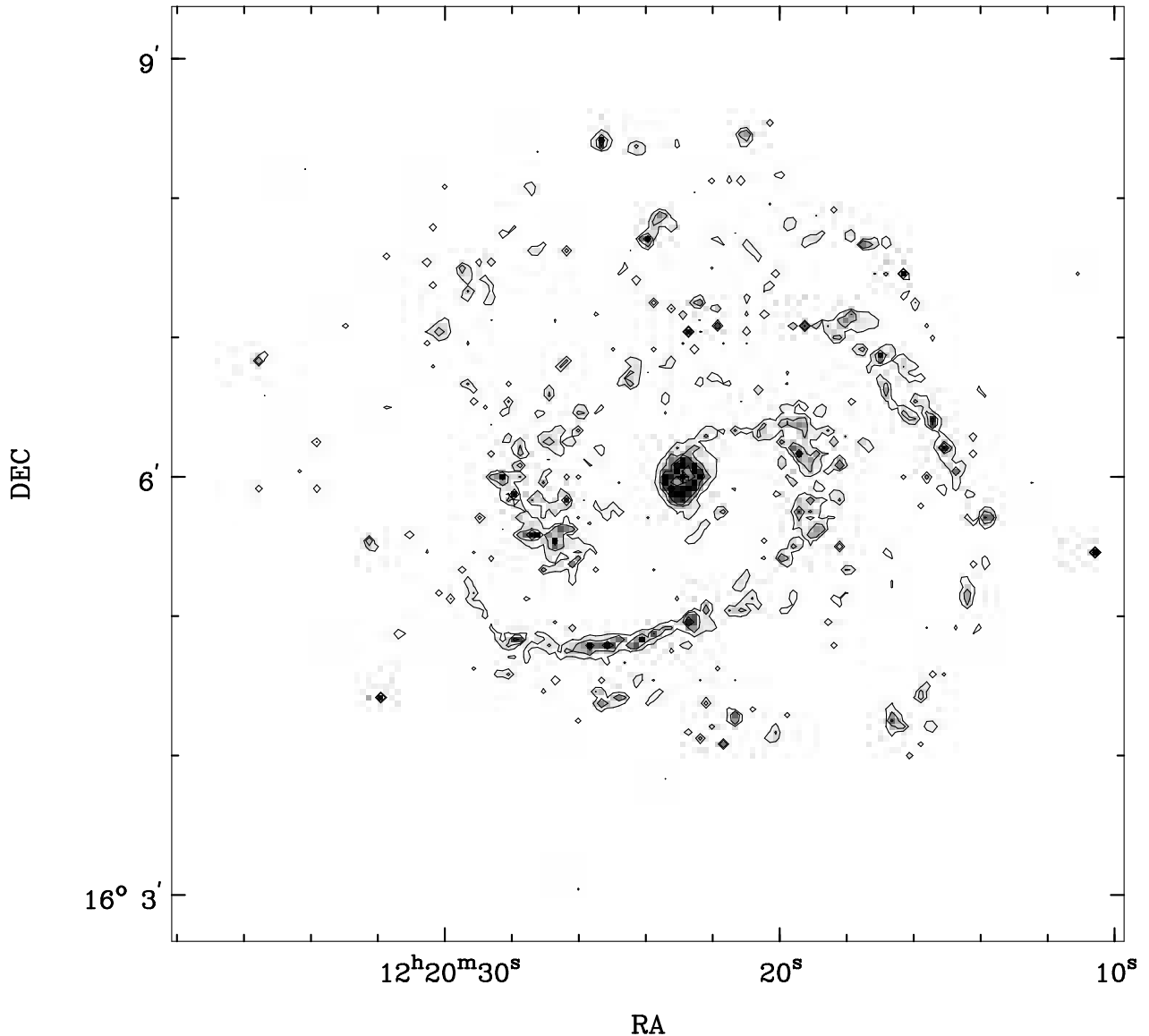


Figure 1. H α continuum-subtracted image of the complete disk of M100. Contour levels are 0.76, 2.3, 6.8, 20.4 and $40.8 \times 10^{36} \text{ erg s}^{-1} \text{ pxl}^{-1}$, grey scales range from 0.57 to $9.5 \times 10^{36} \text{ erg s}^{-1} \text{ pxl}^{-1}$.

due to the inclusion of relatively more high- L HII regions. For all fits to the disc LF, the range over which the fit was made (indicated in Fig. 2) is $37.9 < \log L < 39.3$. A steepening of the LF at high L , and/or a break or jump in the LF has been observed in a number of spiral galaxies, in all cases near $\log L = 38.7 \text{ erg s}^{-1}$, and has been interpreted in physical terms as a distinction between density and ionization bounded HII regions (Beckman et al. 1998). While such an effect is not immediately obvious in the LF as shown in Fig. 2, a more detailed discussion of the possible detection in the data set for M100 is given in Paper II (Rozas et al., in preparation).

4.2 Arm and interarm LFs

Fig. 3 shows the separate LFs for the arm and interarm parts of the disc of M100. The shapes of both the arm and interarm LF are very similar to that of the disc LF discussed before. Fits to the slopes of the arm and interarm HII region LFs yield $a = -2.07 \pm 0.04$ (arm) and $a = -2.18 \pm 0.21$ (interarm), fitting over ranges of $37.9 < \log L < 39.3$ and $37.5 < \log L < 38.5$, respectively. The arm and interarm LF slopes can thus not be considered different, given the errors in the fits. It is difficult to determine what range in $\log L$ is best for use in the fitting, especially for the interarm LF, but the arm and interarm slopes will not be significantly different for any reasonable choice of range. Cepa & Beckman (1990a) concluded from fits to LFs, derived from their list of 456 HII regions as catalogued from an H α image of

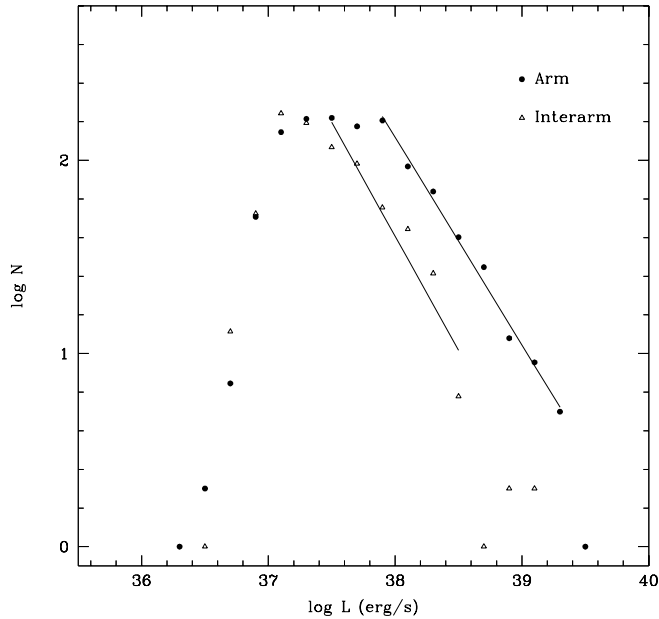


Figure 3. As Fig. 2, now for arm and interarm H II regions separately.

the central 3.1×3.6 part of M100, that arm and interarm LF slopes were slightly different. But they only used less than a quarter of the number of H II regions of the present paper, distributed over a much reduced area of the disc. Furthermore, the errors on their fits, of about ± 0.3 , are large compared to the difference in slope (-2.34 arm, -3.06 interarm). The conclusion must be that their difference is not significant, but does indicate the trend also found in the present paper, that the interarm LF slope is steeper than the arm LF slope.

When compared to the arm LF, the interarm LF is slightly displaced toward the lower left of the diagram, i.e., toward lower numbers and lower luminosities. However, the fact that the arm and interarm LF slopes are equal is a strong indication that the H II populations in and between the arms are *not* different (see also Section 6).

4.3 Circumnuclear region LF

The CNR in M100 accounts for about 16% of the total H α line flux of the complete galaxy (Knapen et al. 1995a). The H α emission is organised into a pair of tightly wound spiral armlets (Knapen et al. 1992, 1995a,b). When attempting to catalogue the individual H II regions here, this large flux concentrated in a relatively small area translates into a crowding problem. On the one hand, the area taken up by the many luminous H II regions precludes detection of the less luminous H II regions, whereas on the other hand, a luminous H II region may in fact be a group of smaller H II regions which is not resolved. These problems were also encountered in especially arm regions of spiral discs, but in the CNR they are much more prominent. I did catalogue the H II regions in the CNR however, and list 98 of them in the (electronically) published catalogue.

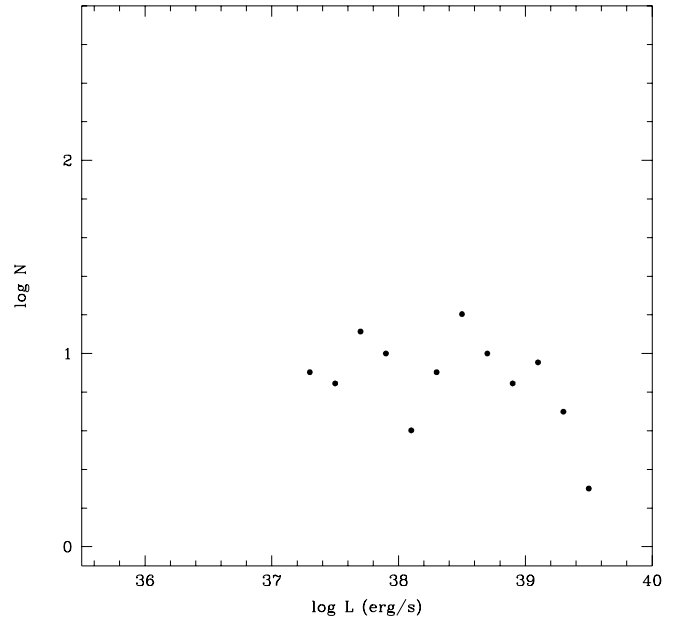


Figure 4. As Fig. 2, now for the H II regions in the CNR of M100 (inner $\sim 25''$).

The resulting CNR H II region LF is shown in Fig. 4. As expected, it shows a prominent H II region population at high luminosities, whereas the low end of the LF is underpopulated to a large extent when compared with e.g. the disc LF. It is possible that smaller H II regions are indeed less numerous in the CNR, when they would be swept up into larger H II regions, but given the observational difficulties described above this cannot be proven here.

4.4 LFs as a function of radius

The large number of H II regions in the catalogue of M100 allowed me to perform a novel type of analysis: to study the detailed radial dependence of the LFs in the disc. There are a number of reports in the literature on LFs in the “inner” and “outer” parts of discs (e.g. Kennicutt et al. 1989; Rand 1992; Knapen et al. 1993a; Banfi et al. 1993), where the division between these sections is usually placed around $0.5 R_{25}$. Rand (1992) reported different slopes for inner and outer parts of the disc of M51, but in the other cases *no* significant differences were found.

Fig. 5 shows the results of the more objective and detailed analysis made possible by the number of almost 2000 H II regions in the M100 catalogue. I constructed LFs, exactly in the same way as done before for e.g. the whole disc, for nine different ranges or bins of deprojected distance from the centre r_d , with width $25''$, and starting at $r_d = 0''$ (central position). The last bin includes all H II regions lying further from the centre than $200''$. Total numbers of H II regions included in each radial bin are decent in all cases except the last two. Table 2 lists the number of H II regions and the fitted LF slope and error for each radial bin, as well as the range in L used for the fit.

I fitted slopes to the LFs in each radial bin. As before,

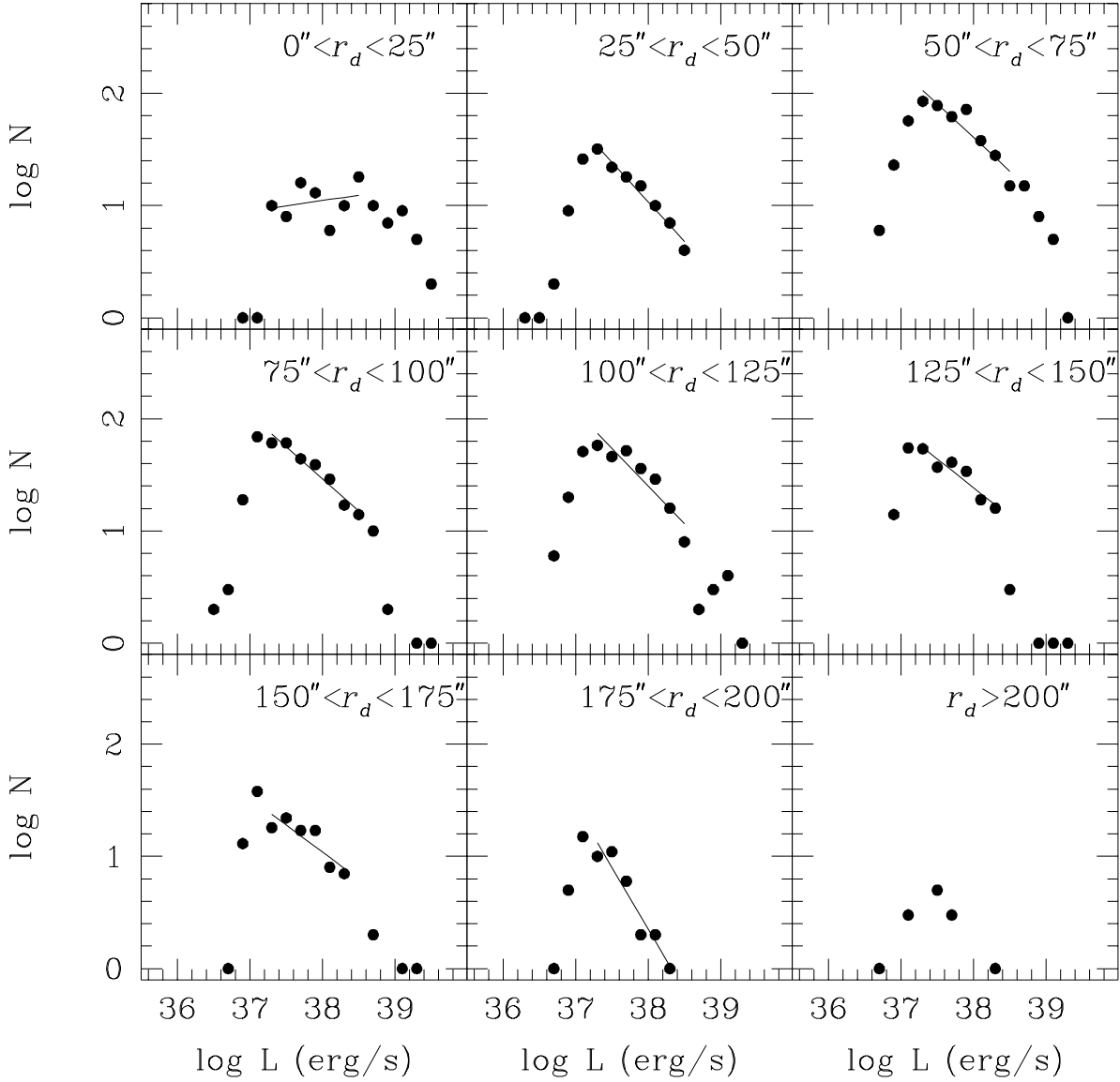


Figure 5. As Fig. 2, but for HII regions within ranges of increasing deprojected distance from the centre (bins are 25'' wide). The appropriate distance range for each LF is indicated in the upper right corner of each panel.

Table 2. LF slopes as function of radius. L is in erg s^{-1} .

Radial bin (")	Central r_d (")	No.	Fitted range ($\log L$)	LF slope a
0–25	12.5	116	37.3–38.5	-0.91 ± 0.17
25–50	37.5	147	37.3–38.5	-1.71 ± 0.05
50–75	62.5	493	37.3–38.5	-1.60 ± 0.11
75–100	87.5	373	37.3–38.5	-1.57 ± 0.06
100–125	112.5	332	37.3–38.5	-1.67 ± 0.12
125–150	137.5	276	37.3–38.3	-1.51 ± 0.09
150–175	162.5	145	37.3–38.3	-1.48 ± 0.14
175–200	187.5	53	37.3–38.5	-2.10 ± 0.16
200–225	212.5	13	–	–

the choice of what range in $\log L$ to include in the fit is somewhat subjective and can directly influence the results,

so I chose to use exactly the same range in all cases (with the exception of radial bins $125'' < r_d < 150''$ and $175'' < r_d < 200''$, where the inclusion of the last point leads to an unrealistic fit to the data set, and for bin $150'' < r_d < 175''$ where there is no data point for $\log L = 38.5$).

The results are listed in Table 2 and plotted as a function of r_d in Fig. 6. Fig. 6 also shows the fit to the radial behaviour of the LF slopes. The LF slopes become shallower with increasing r_d , although this is hardly significant taking the errors on the fits into account. Two discrepant values of the fitted slope occur for the first radial bin, $r_d < 25''$, and for bin no. 8, $175'' < r_d < 200''$. In the first bin, the LF is more or less the LF as derived before for the CNR, which is basically flat up to very high L . The small number of HII regions in bin no. 8 is probably the cause of the deviant LF slope in that bin.

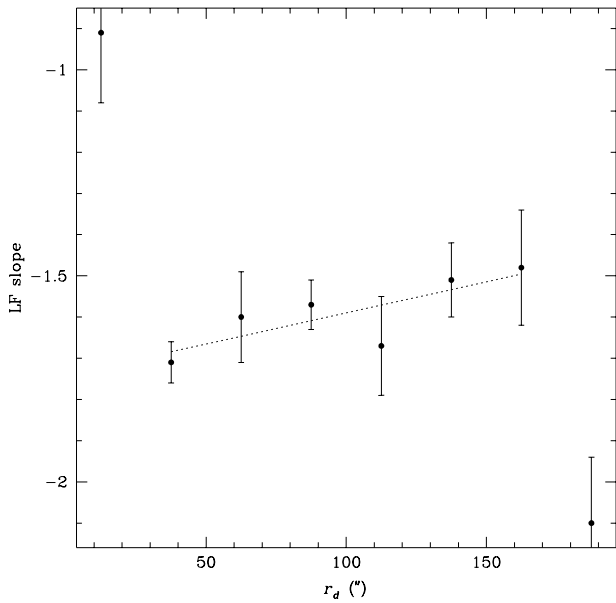


Figure 6. Values of the LF slopes fitted to the LFs shown in Fig. 5, plotted as a function of deprojected distance from the centre (the central distance value of each bin was used). Dashed line indicates best fit to the data points, and range in distance used for the fit.

5 DIAMETER AND RADIAL DISTRIBUTIONS

5.1 Diameter distribution

The integral diameter distribution of H II regions in spiral galaxies usually follows an exponential law:

$$N(> D) = N_0 e^{-D/D_0}$$

with $N(> D)$ the total number of H II regions with diameters larger than D (van den Bergh 1981; Hodge 1987; Ye 1992). The slope of the diameter distribution is correlated with the luminosity of the galaxy (Hodge 1987; see also Rozas et al. 1996b), and the slopes tend to be steeper for H II regions located between the spiral arms than for those within them in the few cases where this has been explicitly studied (Hodge 1987; Knapen et al. 1993a).

The integral diameter distribution of the H II regions in the disc of M100 is shown in Fig. 7 (full dots). Apart from the first point, and the last three points in the Figure, the data are fitted very well with an exponential of the type described above. As usual, the fit to the data points is indicated in the Figure. I also show integral diameter distributions for the H II regions in the CNR (open circles in Fig. 7), and in the arm and interarm areas of the disc separately (Fig. 8). In all cases the data points can be well fitted with an exponential of the type described above. The fitted values to the slopes are $D_0 = 74 \pm 2$ pc and $N_0 = (4.27 \pm 0.37) \times 10^3$ for the whole disc, 48 ± 2 pc and $(0.66 \pm 0.08) \times 10^3$ for the CNR H II regions only, and 78 ± 2 pc and $(2.52 \pm 0.19) \times 10^3$; and 65 ± 3 pc and $(1.90 \pm 0.34) \times 10^3$ for the arm and interarm H II regions, respectively.

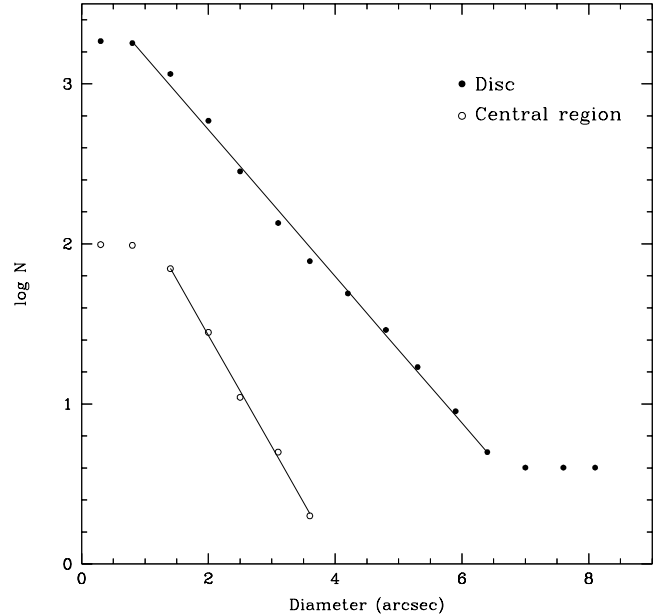


Figure 7. Integral diameter distribution for the H II regions in the disc of M100 (but excluding those in the CNR; filled dots), and in the CNR (open symbols). Lines indicate exponentials fitted to the data points, where the extent of the plotted line indicates the data points used in the fit.

The smaller size scale in the interarm region could be due to evolutionary effects, the interarm H II regions being more evolved (Oey & Clarke 1998) and smaller since their Stromgren sphere will have shrunk. More likely, however, the smaller interarm value for D_0 is due to the fact that in the arms H II regions overlap more often, and determining the diameters of the smaller H II regions will be more difficult.

The disc value derived here is significantly smaller than values derived by other authors: after correcting to the distance to M100 as used in the present paper, Arsenault et al. (1990) find $D_0 = 112$ pc, Cepa & Beckman (1990a) $D_0 = 128$ pc, and Banfi et al. (1993) $D_0 = 165$ pc (no errors given). Especially in the case of Banfi et al. (1993), who catalogue only 83 H II regions for M100, the larger values found in the literature can be explained by a smaller number of H II regions used as input for the diameter determination. This is usually a result of a combination of lower resolution and lower sensitivity in the H α images, leading to overestimates of the diameters of H II region complexes which would have been resolved using better imaging. The value of $D_0 = 74 \pm 2$ pc places M100 below the relation found by Hodge (1987) between the absolute magnitude M_B and the H II region size scale D_0 for spiral galaxies. However, the effects on systematic and instrumental influences on the individual data points in the M_B vs. D_0 relation, as outlined above, remain to be investigated.

The diameter distribution for the CNR shows a steeper slope than any of the others, and the interarm slope is significantly steeper than the arm slope, following the trend set in earlier work (Hodge 1987; Knapen et al. 1993a). However, especially in the CNR the diameter determination may be less reliable due to crowding, making it harder to determine

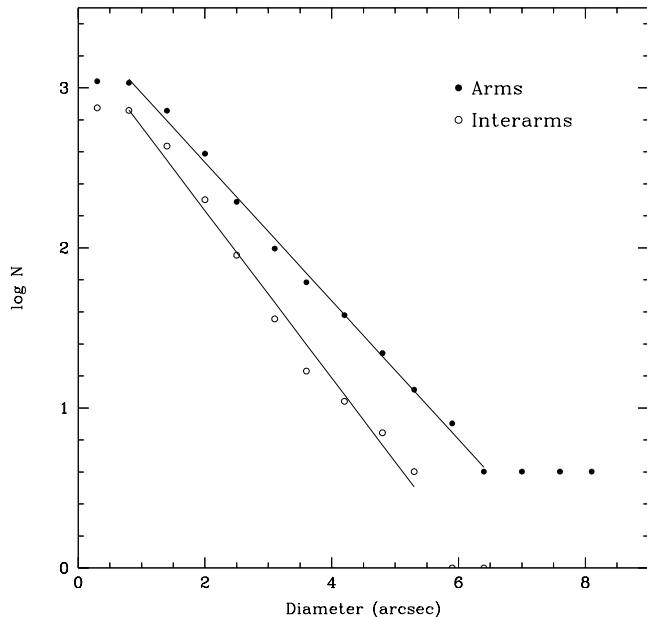


Figure 8. As Fig. 7, now for arm (filled dots) and interarm (open symbols) H II region populations separately.

the true extent of the H II regions, and thus underestimating the diameters of many of them. On the other hand, one would expect the same effect to have more impact on the arm than on the interarm H II regions, so the shallower slope for the arm H II regions may in fact be a lower limit to the true slope. Finally, the fact that the LFs are very similar for the arm and interarm H II region populations means that interarm H II regions will have, on average, higher surface brightnesses than arm H II regions (see also Knapen et al. 1993a).

5.2 Radial distribution

Fig. 9 shows the number density of H II regions in M100 as a function of deprojected distance from the centre. The number density is defined as the number of H II regions in annular bins of $10''$ width, normalized by the area in which they are found. Number densities are shown for all H II regions in the catalogue, and for arm and interarm H II regions separately. At the innermost data point the number density is in fact 9.8, a high value caused by the large number of H II regions in the CNR. The distribution is characterised by a number of components that can be easily recognised morphologically, e.g. on the grey-scale image of Fig. 1, namely the strongly star-forming CNR ($0'' < r_d < 20''$), the bar which is mostly devoid of massive SF ($20'' < r_d < 50''$), the star-forming spiral arms ($50'' < r_d < 160''$), and the outer disc, with only sporadically occurring H II regions ($160'' < r_d < 240''$). Note that these components were also identified by Knapen & Beckman (1996) from a radial H α profile. Within the spiral arm region, the highest number density of H II regions occurs in a relatively small area with radii between some $50''$ and $80''$. This is the region where the large star-forming complexes are located which can be seen in e.g. Fig. 1 near

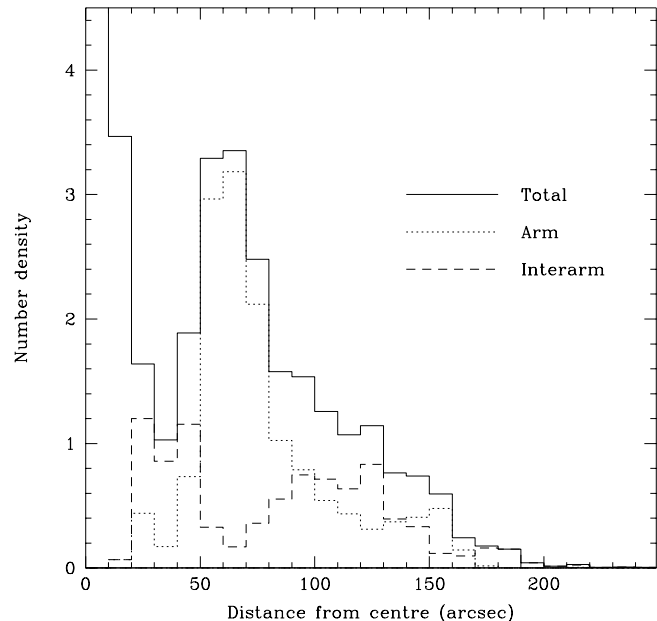


Figure 9. Number density distribution for all H II regions catalogued in M100 (including the CNR; drawn line), and for arm (dotted line) and interarm (dashed line) H II region populations separately. The number density in the innermost bin is 9.8.

the ends of the bar, and especially in the spiral arm part south of the nuclear region, connecting with the western end of the bar. The separate arm and interarm H II region distribution shows less interarm H II regions in the crowded areas in the arms ($50'' < r_d < 80''$), and more interarm than arm H II regions in the bar region and at specific radii further out in the disc (e.g. $100'' < r_d < 130''$).

In general, the number density distribution is similar to the radial profile as shown by Knapen & Beckman (1996; their Fig. 4), where the radial H α profile is plotted logarithmically. Note that the outermost H II regions occur at distances $r_d > D_{25}/2$ from the centre, the outermost one lies near $r_d \sim 245''$.

6 DISCUSSION AND SUMMARY

In this paper, I present a detailed study of a new, high-quality H α continuum-subtracted image of the grand-design spiral galaxy M100. From the image, I have catalogued a total of 1948 individual H II regions, and tabulated basic properties for each H II region: position with respect to the centre, radius, and integrated flux. A substantial part of the paper is devoted to deriving LFs for the complete sample of H II regions, and sub-samples of the whole set, defined on the basis of the location of the H II regions in the galaxy. Following previous work, separate LFs for arm, interarm and CNR H II regions were derived, but the huge number of individual H II regions available also made it possible, for the first time, to derive a set of nine LFs for H II regions at increasing distance from the centre.

The total LF (Fig. 2) shows the by now well-known shape and characteristics (see e.g. Kennicutt et al. 1989;

Rand 1992; Knapen et al. 1993a; and Rozas et al. 1996a for LFs of other galaxies). A sharp cut-off at low luminosities indicates our detection limit, while the slope at luminosities larger than the completeness limit can be well fitted with a power law, giving an LF slope of $a = -2.17 \pm 0.04$, well within the limits established in the previous works for a galaxy of this morphological type. I fail to detect a significant difference between the LF slopes for the arm and interarm populations of H II regions. As discussed before, this does not contradict published results by Cepa & Beckman (1990a) who studied the central part of M100.

This adds yet another galaxy to the list of those that do not show significantly different arm vs. interarm H II region LF slopes. Rand (1992) did find significantly different slopes in M51, a galaxy with a relatively small number of interarm H II regions and strong density waves in its disc, as did Kennicutt et al. (1989) for a number of their galaxies, although the latter result was based on observational data of considerably lower quality than those used in later work. Kennicutt et al. (1989) present a combined result for five galaxies, which shows slightly steeper slopes for interarm H II regions (no fits to the slopes or estimates of errors are given so the significance of the result can not be easily compared with those for other galaxies). Rand (1992) interpreted the significantly different arm-interarm LF slopes in terms of a different molecular cloud mass spectrum, but Oey & Clarke (1998) explain such differences in general by evolutionary effects and the maximum number of ionizing stars per cluster. Knapen et al. (1993a) and Rozas et al. (1996a) did not find significant arm-interarm LF slope differences in the 5 galaxies they studied.

In most cases where interarm and arm LF slopes have been considered, the interarm LF slopes are marginally steeper than arm LF slopes, although not significantly so. But for two of the four galaxies studied by Rozas et al. (1996a) the arm LF slope is steeper, so even *if* the trend noticed exists, it is not unique. The only way forward is to observe more galaxies, but significantly different LF slopes in arm and interarm environments can be ruled out based on the existing data, with the exception of one galaxy (M51).

This implies that the observed occurrence of many large H II regions in the spiral arms does not indicate a preference for the larger H II regions to form there, but merely a statistical effect: there are more H II regions in the arms, so there will also be more large ones (e.g. Elmegreen 1993). The spiral density waves which must be present in grand-design galaxies thus only re-organize the material from which the stars form, and the SF, into the arms. This agrees with the observed lack of correlation between the SF rates per unit area and arm class (Elmegreen & Elmegreen 1986)[†]. But equal arm and interarm H II region LF slopes seem harder to unite with the observed higher massive SF efficiencies within the arms as compared to outside the arms (Cepa & Beckman 1990b; Knapen et al. 1992, 1996), which are *prima facie* evidence for triggering of the massive SF within the arms, presumably by the density wave. The overall conclusion must be that *whereas the density wave organizes the material into*

the arms, and enhances (triggers) the massive SF, *it does not in fact change the mass distribution of the star-forming molecular clouds*, and thus of the statistical properties of the H II region population. It just allows more of basically the same H II regions to start emitting in the arms.

There is a slight change in the LF slopes with increasing radius (Fig. 6), with slopes decreasing (becoming shallower) with increasing radius. Note that Rand (1992) found a steeper slope in the outer part of the disc of M51 than in the inner part, a result which goes in the opposite direction as the trend found here for M100. The result for M100 would indicate the presence of relatively more large H II regions at larger distances from the centre, or, following the results of the theoretical treatment by Rozas (1996), a shallower IMF further out in the disc. Alternatively, evolutionary effects in the H II region population, as described by e.g. Oey & Clarke (1998), could be responsible for the observed effect. This is an interesting point which should be followed up by more extensive study, preferably through spectroscopic observations of decent numbers of H II regions at varying distances from the centre.

Acknowledgements

I thank J.E. Beckman for his continuing support of and interest in this work, and M.S. Oey and C.H. Heller for helpful discussion. N. Arnth-Jensen wrote the first version of most of the Fortran programmes I used. This paper is based on observations obtained at the William Herschel Telescope, operated on the island of La Palma by the Royal Greenwich Observatory in the Spanish Observatorio del Roque de los Muchachos of the Instituto de Astrofísica de Canarias. Financial support from the British Council and the Spanish Acciones Integradas Programme, and from the Spanish DGCYT, Grant No. PB94-1107, is acknowledged.

REFERENCES

- Arsenault, R., Roy, J.-R. & Boulesteix, J. 1990, A&A 234, 23
 Anderson, S., Hodge, P.W. & Kennicutt, R.C. 1983, ApJ 265, 132
 Banfi, M., Rampazzo, R., Chincarini, G. & Henry, R.B.C. 1993, A&A 280, 373
 Beckman, J.E., Rozas, M., Zurita, A. & Knapen, J.H. 1998, ApJ, submitted
 Cepa, J. & Beckman, J.E. 1989, A&AS 79, 41
 Cepa, J. & Beckman, J.E. 1990a, A&AS 83, 211
 Cepa, J. & Beckman, J.E. 1990b, ApJ 349, 497
 Cepa, J., Beckman, J.E., Knapen, J.H., Nakai, N. & Kuno, N. 1992, AJ 103, 429
 Crocker, D.A., Baugus, P.D. & Buta, R. 1996, ApJS 105, 353
 de Vaucouleurs, G., de Vaucouleurs, A., Corwin, H.G., Buta, R.J., Paturel, G., Fouqué, P., 1991, Third Reference Catalogue of Bright Galaxies, Springer, New York
 Elmegreen, D.M. 1993, in: *Star Formation, Galaxies and the Interstellar Medium*, Eds. Franco, J., Ferrini, F. & Tenorio-Tagle, G., University Press, Cambridge, p.108
 Elmegreen, B.G. & Elmegreen, D.M. 1986, ApJ 311, 554
 Evans, I.N., Koratkar, A.P. Storchi-Bergman, T., Kirkpatrick, H., Heckman, T.M. & Wilson, A.S. 1996, ApJS 105, 93
 Ferrarese, L. et al. 1996, ApJ 464, 568
 González Delgado, R.M., Pérez, E., Tadhunter, C., Vilchez, J.M. & Rodríguez Espinosa, J.M. 1997, ApJS 108, 155
 Hodge, P.W. 1987, PASP 99, 915
 Hodge, P.W. & Kennicutt, R.C. 1983, AJ 88, 296
 Hodge, P.W. & Miller, B.W. 1995, ApJ 451, 176

[†] The SF rate per unit area does vary strongly with morphological type, see Kennicutt & Kent (1983) or the review by Kennicutt (1992), and the references therein.

- Kennicutt, R.C. 1992, in: *Star Formation in Stellar Systems*, Eds. G. Tenorio-Tagle, M. Prieto & F. Sánchez, University Press, Cambridge, p. 191
- Kennicutt, R.C. & Kent, S.M. 1983, AJ 88, 1094
- Kennicutt, R.C., Edgar, B.K. and Hodge, P.W. 1989, ApJ 337, 761
- Knapen, J.H., Beckman, J.E., Cepa, J., van der Hulst, J.M. & Rand, R.J. 1992, ApJL 385, L37
- Knapen, J.H., Arnth-Jensen, N., Cepa, J. & Beckman, J.E. 1993a, AJ 106, 56
- Knapen, J.H., Cepa, J., Beckman, J.E., del Rio, M.S. & Pedlar, A. 1993b, ApJ 416, 563
- Knapen, J.H., Beckman, J.E., Shlosman, I., Peletier, R.F., Heller, C.H. & de Jong, R.S. 1995a, ApJL 443, L73
- Knapen, J.H., Beckman, J.E., Heller, C.H., Shlosman, I. & de Jong, R.S. 1995b, ApJ 454, 623
- Knapen, J.H., & Beckman, J.E. 1996, MNRAS 283, 251
- Knapen, J.H., Beckman, J.E., Cepa, J. & Nakai, N. 1996, A&A, 308, 27
- Oey, M.S. & Clarke, C.J. 1998, AJ, in press
- Rand, R.J. 1992, AJ 103, 815
- Rozas, M. 1996, PhD thesis, Univ. La Laguna
- Rozas, M., Beckman, J.E., & Knapen, J.H. 1996a, A&A 307, 735
- Rozas, M., Knapen, J.H., & Beckman, J.E. 1996b, A&A 312, 275
- Ryder, S.D. & Dopita, M.A. 1993, ApJS 88, 415
- Tsvetanov, Z.I. & Petrosian, A.R. 1995, ApJS 101, 287
- Van den Bergh, S. 1981, AJ 86, 1464
- Ye, T. 1992, MNRAS 255, 32

This paper has been produced using the Royal Astronomical Society/Blackwell Science L^AT_EX style file.